Converting one photon into two via four-wave mixing in optical fibers

Audrey Dot,[1,*] Evan Meyer-Scott,[1] Raja Ahmad,[2] Martin Rochette,[2] and Thomas Jennewein[1]

[1]*Institute for Quantum Computing and Department of Physics and Astronomy, University of Waterloo, 200 University Avenue West, Waterloo, Ontario, Canada N2L 3G1*

[2]*Department of Electrical and Computer Engineering, McGill University, 3480 University Street, Montréal, Québec, Canada H3A 2A7*

Observing nonlinear optical quantum effects or implementing quantum information protocols using nonlinear optics requires moving to ever-smaller input light intensities. However, low light intensities generally mean weak optical nonlinearities, which are inadequate for many applications. Here we calculate the performance of four-wave mixing in various optical fibers for the case where one of the input beams is a single photon. We show that in tapered chalcogenide glass fibers (microwires) a single photon plus strong pump beam can produce a pair of photons with a probability of 0.1%, much higher than in previous work on bulk and wave-guided crystal sources. Such a photon converter could be useful for creating large entangled photon states, for performing a loophole-free test of Bell's inequalities, and for quantum communication.

PACS number(s): 42.65.Lm, 42.50.Nn, 42.65.Wi

I. INTRODUCTION

Pairs of photons created via spontaneous parametric down-conversion (SPDC) [1] or spontaneous four-wave mixing (FWM) [2] in a nonlinear optical material with a high-intensity pump laser have been used in many experiments in quantum optics, quantum metrology, and optical quantum information processing. Interest is increasingly converging on using SPDC or FWM in later stages of quantum information protocols, rather than just initial sources of photons [3–5]. This requires operation with very low intensity input states, including converting a single photon into a pair.

Should an efficient one-to-two-photon conversion be realized, one important application is the entangling of three or more photons [6,7]. These large entangled photon states are useful in quantum communication protocols [8,9] and allow fundamental tests of quantum mechanics [7,10,11]. Increased efficiency in converting single photons to pairs would allow larger states to be generated, with greater speed. Single-photon conversion could also be used for heralding photons after long-distance transmission to close the Bell test detection loophole [12] and for device-independent quantum key distribution [13]; any improvement in conversion efficiency directly increases the communication rates. Finally, if efficient enough, single-photon conversion could also be used directly in quantum computing as a two-qubit gate [14].

The key challenge in converting a single photon into a pair is the low efficiency of nonlinear optical processes at ultralow power. In principle, standard SPDC or FWM sources could be used, but the low efficiency (less than 10^{-5}) limits the single-photon conversion to rates too low to be useful [15]. Therefore we consider here specialty fiber media, which we show can result in large conversion efficiencies thanks to long length, small core size, and high nonlinearity.

We present complete calculations and simulations of FWM between a strong pump and a single photon as illustrated schematically in Fig. 1. First we set up the theoretical framework by extending the quantum theory of nondegenerate FWM [16,17] to the single-photon pump case. Then we apply

the expressions to birefringent silica fibers, microstructured silica fibers, and chalcogenide microwires to find the spectra and conversion efficiency of the generated two-photon states.

II. QUANTUM THEORY OF FWM PUMPED BY A SINGLE PHOTON AND STRONG LASER

A. Equations of motion for a $\chi^{(3)}$ nonlinear medium

We determine the operator evolution of a system consisting of a strong pump beam and a single photon entering a nonlinear, dispersive, single-mode fiber and undergoing four-wave mixing and phase modulation as in Fig. 1. We proceed in the Heisenberg representation by solving the equation of motion for the field amplitude operators [18]. The two pumping fields are considered to be monochromatic or quasimonochromatic, and we include self- and cross-phase modulation but not parasitic effects such as Raman scattering and multiphoton absorption due to the low power of the inputs. We stay in the low-gain regime, which means that only spontaneous FWM (also called four-photon scattering) is studied. This approximation stands if the total probability of generating a photon pair during the interaction is much lower than 1 and certainly holds since one of our pumps is a single photon.

The field is quantized in one dimension in a length large enough for the electric field to be written in the continuous limit [19]. We then choose, for convenience, to write this field in the frequency space as a sum of its space-dependent spatial mode operators, an approach introduced in Ref. [18]. The quantization time T, equal to the quantization length divided by the speed of light, is then the time periodicity of the field, and the density of the frequency space is $\delta\omega = 2\pi/T$. T has to be long enough to allow the writing of the frequency modes in the continuous limit. The electric field is then

$$\hat{\vec{E}}(r,t) = \sum_{j=x,y} \left(F(x,y)\sqrt{\frac{\hbar}{2\varepsilon_0 c}}\frac{1}{\sqrt{2\pi}} \right.$$

$$\left. \times \int d\omega \sqrt{\frac{\omega}{n_j(\omega)}}\hat{a}_j(\omega,z)e^{-i\omega t} + \text{H.c.} \right) \vec{e}_j, \quad (1)$$

where the frequency integral runs from 0 to $+\infty$ and H.c. stands for the Hermitian conjugate. $F(x,y)$, with

*audreyddot@gmail.com
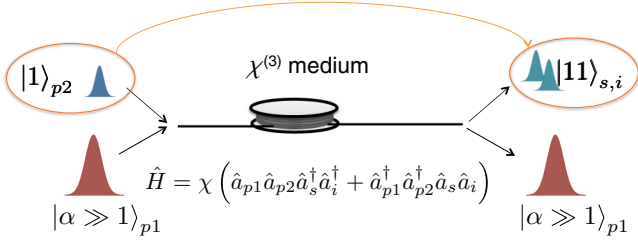
FIG. 1. (Color online) Four-wave mixing (FWM) with single-photon and strong-pump inputs. The toy Hamiltonian with interaction parameter χ illustrates the processes, but the full development is given in the text.

$\iint |F(x,y)|^2\,dx\,dy = 1$, is the transverse distribution of the fiber mode. The unit vectors $\vec{e}_j$ describe the field's polarization, and $n_j(\omega)$ is the effective index of refraction for the fiber mode of frequency ω and polarization j. Since we are in the continuous limit, we approximated the discrete longitudinal modes of a laser cavity by continuous-mode annihilation operators $\hat{a}_j(\omega,z)$ with units of inverse square-root frequency [19]. They follow the commutation relations $[\hat{a}_j(\omega,z),\hat{a}_{j'}^\dagger(\omega',z)] = \delta(\omega - \omega')\delta_{jj'}$, with Dirac delta $\delta(\omega - \omega')$ and Kroenecker delta $\delta_{jj'}$.

These operators $\hat{a}_j(\omega,z)$ and the quantum state of the system $|\psi\rangle$ provide complete knowledge about the state as a function of propagation distance z, which allows us to extract the efficiency of single-photon-to-pair conversion. In the Heisenberg representation, $|\psi\rangle$ is constant, and we only need to solve for the evolution of the annihilation operators.

If we consider only one polarization component, the propagating field can be simplified into

$$\hat{E}(z,t) = \sqrt{\frac{\hbar}{4\pi\varepsilon_0 c A_{\text{eff}}}} \int d\omega \sqrt{\frac{\omega}{n(\omega)}} \hat{a}(\omega,z)e^{-i\omega t} + \text{H.c.}$$
$$= \hat{E}^{(+)}(z,t) + \hat{E}^{(-)}(z,t), \quad (2)$$

where the transverse modal distribution was also simplified using the effective area of the fiber mode $A_{\text{eff}} = \frac{1}{\iint |F(x,y)|^4 dx dy}$, which is taken to be the same for all the frequency components in the fiber.

The evolution equation of the annihilation operators can be given by

$$\frac{\partial \hat{a}(\omega,z)}{\partial z} = \frac{i}{\hbar}[\hat{a}(\omega,z),\hat{G}(z)], \quad (3)$$

where the momentum operator $\hat{G}$ is given by integration over the cross-sectional area of the momentum that flows during the quantization time.

$$\hat{G}(z) = \int_{A_{\text{eff}}} dS \int_0^T dt\, \hat{D}^{(-)}(z,t)\hat{E}^{(+)}(z,t) + \text{H.c.}, \quad (4)$$

where $\hat{D}(z,t) = \varepsilon_0 \hat{E}(z,t) + \hat{P}(z,t)$ is the electric displacement operator. The polarization operator is defined by

$$\hat{P}(z,t) = \sum_{n \geqslant 1} \varepsilon_0 \chi^{(n)} \hat{E}^n(z,t) = \hat{P}_l(z,t) + \hat{P}_{nl}(z,t), \quad (5)$$

which is the sum of the linear polarization $\hat{P}_l(z,t)$ given by $\varepsilon_0\chi^{(1)}(\omega)\hat{E}(r,t)$ and the nonlinear polarization $\hat{P}_{nl}(z,t)$ of higher orders. We can thus separate $\hat{G}(z)$ into linear and nonlinear parts as $\hat{G}(z) = \hat{G}_l(z) + \hat{G}_{nl}(z)$, driven by corresponding linear and nonlinear polarizations.

The linear evolution of the momentum operator is obtained from Eqs. (2), (4), and (5) as (see Appendix A)

$$\hat{G}_l(z) = \int d\omega \hbar\beta(\omega)\hat{a}^\dagger(\omega,z)\hat{a}(\omega,z), \quad (6)$$

with the propagation constant $\beta(\omega) = \frac{n(\omega)\omega}{c}$. The linear evolution of any annihilation operator can thus be deduced from Eqs. (3) and (6) as

$$\hat{a}_l(\omega,z) = \hat{a}_0(\omega,z)e^{i\beta(\omega)z}. \quad (7)$$

The nonlinear evolution [contained in $\hat{a}_0(\omega,z)$] can be found similarly from the nonlinear evolution of the momentum. $\hat{G}_{nl}$ can be decomposed into two parts as $\hat{G}_{nl}(z) = \hat{G}_{nl}^{\text{FWM}}(z) + \hat{G}_{nl}^{\text{ph mod}}(z)$ (see Appendix A), one giving FWM and the other phase modulation.

The two pumping fields, of frequencies $\omega_{p1,2}$, are considered to be monochromatic or quasimonochromatic and perfectly overlapping in time and have the same spectral bandwidth $\delta\omega_p$ with $\delta\omega_p/\omega_{p1,2} \ll 1$. It is convenient to choose the quantization time as the Fourier transform of the pulses' spectral width, $T = 2\pi/\delta\omega_p$. The frequency-space density is therefore $\delta\omega = \delta\omega_p$. For monochromatic pumps, this quantization time, as well as the pulse duration, is infinite.

The FWM part of the momentum operator is (see Appendix A)

$$\hat{G}_{nl}^{\text{FWM}}(z) = 3\chi^{(3)}\frac{\hbar^2}{\varepsilon_0 c^2 A_{\text{eff}} T}\frac{2\pi}{T}$$
$$\times\left[\int d\omega \sqrt{\frac{\omega\omega_{p1}\omega_{p2}(\omega_{p1}+\omega_{p2}-\omega)}{n(\omega)n(\omega_{p1})n(\omega_{p2})n(\omega_{p1}+\omega_{p2}-\omega)}}\right.$$
$$\times \hat{a}_0^\dagger(\omega,z)\hat{a}_0^\dagger(\omega_{p1}+\omega_{p2}-\omega,z)$$
$$\left.\times \hat{a}_0(\omega_{p1},z)\hat{a}_0(\omega_{p2},z)e^{-i\Delta kz} + \text{H.c.}\right], \quad (8)$$

with $\Delta k = \beta(\omega) + \beta(\omega_{p1} - \omega_{p2} - \omega) - \beta(\omega_{p1}) - \beta(\omega_{p2})$, where the integral over ω covers the whole positive spectrum except the two injected frequencies. The two creation operators $\hat{a}_0^\dagger(\omega,z)\hat{a}_0^\dagger(\omega_{p1}+\omega_{p2}-\omega,z)$ indicate that output photons can only be created in pairs, with correlated frequencies ω and $\omega_{p1}+\omega_{p2}-\omega$.

The phase modulation part is (see Appendix A)

$$\hat{G}_{nl}^{\text{ph mod}}(z) = 3\chi^{(3)}\frac{\hbar^2}{\varepsilon_0 c^2 A_{\text{eff}} T}\left[\iint d\omega d\omega' \frac{\omega}{n(\omega)}\frac{\omega'}{n(\omega')}\hat{a}_0^\dagger(\omega,z)\hat{a}_0(\omega',z)\hat{a}_0^\dagger(\omega',z)\hat{a}_0(\omega,z)\right.$$
$$\left. -\frac{1}{2}\int d\omega\frac{2\pi}{T}\left(\frac{\omega}{n(\omega)}\hat{a}_0^\dagger(\omega,z)\hat{a}_0(\omega,z)\right)^2\right], \quad (9)$$

with the integrals covering the whole positive spectrum.

We can now derive the evolution of the mode operators from Eq. (3) for any frequency generated in the fiber.

$$\frac{\partial \hat{a}_0(\omega,z)}{\partial z} = 3i\chi^{(3)} \frac{\hbar}{\varepsilon_0 c^2 A_{\text{eff}} T} \left[\frac{2\pi}{T} \sqrt{\frac{\omega \omega_{p1} \omega_{p2}(\omega_{p1}+\omega_{p2}-\omega)}{n(\omega)n(\omega_{p1})n(\omega_{p2})n(\omega_{p1}+\omega_{p2}-\omega)}} \hat{a}_0^\dagger(\omega_{p1}+\omega_{p2}-\omega,z)\hat{a}_0(\omega_{p1},z)\hat{a}_0(\omega_{p2},z)e^{-i\Delta k z} \right.$$

$$\left. + \frac{\omega}{n(\omega)} \int d\omega' \frac{\omega'}{n(\omega')} \left[\hat{a}_0^\dagger(\omega',z)\hat{a}_0(\omega',z) + \frac{1}{2}\frac{T}{2\pi} \right] \hat{a}_0(\omega,z) - \frac{1}{2}\frac{2\pi}{T}\frac{\omega^2}{n(\omega)^2} \hat{a}_0^\dagger(\omega,z)\hat{a}_0(\omega,z)\hat{a}_0(\omega,z) \right]. \tag{10}$$

The first of the two summed terms reflects the evolution by FWM, and the second reflects the self-phase modulation. If we neglect the phase modulation arising from the generated frequencies because they will be much weaker than the pumps, we have, for the generated frequencies,

$$\frac{\partial \hat{a}_0(\omega,z)}{\partial z} = 3i\chi^{(3)} \frac{\hbar}{\varepsilon_0 c^2 A_{\text{eff}} T} \frac{2\pi}{T} \left[\sqrt{\frac{\omega \omega_{p1} \omega_{p2}(\omega_{p1}+\omega_{p2}-\omega)}{n(\omega)n(\omega_{p1})n(\omega_{p2})n(\omega_{p1}+\omega_{p2}-\omega)}} \hat{a}_0^\dagger(\omega_{p1}+\omega_{p2}-\omega,z)\hat{a}_0(\omega_{p1},z)\hat{a}_0(\omega_{p2},z)e^{-i\Delta k z} \right.$$

$$\left. + \frac{\omega}{n(\omega)} \left[\frac{\omega_{p1}}{n(\omega_{p1})} \hat{a}_0^\dagger(\omega_{p1},z)\hat{a}_0(\omega_{p1},z) + \frac{\omega_{p2}}{n(\omega_{p2})} \hat{a}_0^\dagger(\omega_{p2},z)\hat{a}_0(\omega_{p2},z) + \frac{1}{2}\frac{\omega}{n(\omega)}\frac{T}{2\pi} \right] \hat{a}_0(\omega,z) \right]. \tag{11}$$

For the incoming pump frequencies the evolution is given by

$$\frac{\partial \hat{a}_0(\omega_j,z)}{\partial z} = 3i\chi^{(3)} \frac{\hbar}{\varepsilon_0 c^2 A_{\text{eff}} T} \left[\int d\omega \sqrt{\frac{\omega \omega_j \omega_k(\omega_j+\omega_k-\omega)}{n(\omega)n(\omega_j)n(\omega_k)n(\omega_j+\omega_k-\omega)}} \hat{a}_0(\omega,z)\hat{a}_0(\omega_{p1}+\omega_{p2}-\omega,z)\hat{a}_0^\dagger(\omega_k,z)e^{i\Delta k z} \right.$$

$$\left. + \frac{2\pi}{T}\frac{\omega_j}{n(\omega_j)} \left[\frac{1}{2}\frac{\omega_j}{n(\omega_j)} \hat{a}_0^\dagger(\omega_j,z)\hat{a}_0(\omega_j,z) + \frac{\omega_k}{n(\omega_k)} \hat{a}_0^\dagger(\omega_k,z)\hat{a}_0(\omega_k,z) + \frac{1}{2}\frac{\omega}{n(\omega)}\frac{T}{2\pi} \right] \hat{a}_0(\omega_j,z) \right], \tag{12}$$

with $j,k = $ p1,p2,

Although we are in the quasimonochromatic approximation, the pumps' creation and annihilation operators are not dimensionless for homogeneity with those of the generated modes.

B. Solution for a single photon and a strong pump

To solve Eqs. (11) and (12), the strong pump is taken to be classical $[\hat{a}_0(\omega_{p1},z) \equiv A_{p1}(z)]$ and undepleted $[|A_{p1}(z)|^2 = |A_{p1}(0)|^2]$. The weak pump, p2, has to be kept quantum throughout since it is on the few- or single-photon level. Therefore we can also assume the number of weak-pump photons is negligible compared to the number of strong-pump photons, and so we neglect phase modulation from the weak pump.

We use the standard waveguide nonlinear parameter $\gamma(\omega) = \frac{3\chi^{(3)}\omega}{2\varepsilon_0 c^2 n(\omega)^2 A_{\text{eff}}}$. If all the frequencies are close, we can use the same averaged γ for all the frequency modes, which is commonly used to simplify the notation but is not necessary for the solution [20].

With these approximations the evolution of the strong pump can be simplified from Eq. (12) to

$$\frac{dA_{p1}(z)}{dz} = i\gamma P_1 A_{p1}(z), \tag{13}$$

where we defined the pump peak power as $P_1(z) = \frac{\hbar \omega_{p1} \times N_1(z)}{T} = \frac{2\pi \hbar \omega_{p1}}{T^2}|A_{p1}(z)|^2$. Here $N_1(z) = \frac{2\pi}{T}|A_{p1}(z)|^2$ is the number of pump photons going through a plane at position z per time T. In the undepleted pump approximation, P_1 is independent of z.

Equation (13) is solved as [21]

$$A_{p1}(z) = A_{p1}(0)e^{i\gamma P_1 z}. \tag{14}$$

The evolution of the weak pump can then be simplified from Eq. (12) to

$$\frac{\partial \hat{a}_0(\omega_{p2},z)}{\partial z} = \frac{2i\gamma\hbar}{T} \int d\omega \sqrt{\omega(\omega_{p1}+\omega_{p2}-\omega)} A_{p1}^*(0) e^{-i\gamma P_1 z} \hat{a}_0(\omega,z)\hat{a}_0(\omega_{p1}+\omega_{p2}-\omega,z)e^{i\Delta k z} + 2i\gamma P_1 \hat{a}_0(\omega_{p2},z), \tag{15}$$

and if we choose $A_{p1}^*(0) = A_{p1}(0) = T\sqrt{\frac{P_1}{2\pi\hbar\omega_{p1}}}$, then

$$\frac{\partial \hat{a}_0(\omega_{p2},z)}{\partial z} = 2i\gamma \left[\sqrt{P_1} \sqrt{\frac{\hbar}{2\pi\omega_{p1}}} \int d\omega \sqrt{\omega(\omega_{p1}+\omega_{p2}-\omega)} \hat{a}_0(\omega,z)\hat{a}_0(\omega_{p1}+\omega_{p2}-\omega,z)e^{i(\Delta k - \gamma P_1)z} + P_1 \hat{a}_0(\omega_{p2},z) \right]. \tag{16}$$

We can write this more explicitly by introducing $\zeta_2 = \frac{2\pi\hbar\omega_{p2}}{T^2}$, where $\zeta_2\langle\hat{a}^\dagger(\omega_{p2},0)\hat{a}(\omega_{p2},0)\rangle = P_2$ is the peak power of the weak pump at the medium entrance, with $P_2 = \zeta_2\frac{T}{2\pi}$ in the case of a single-photon pumping. We then have

$$\frac{\partial\hat{a}_0(\omega_{p2},z)}{\partial z} = 2i\gamma\left[\sqrt{P_1}\sqrt{\zeta_2}\frac{2\pi}{T}\int d\omega\hat{a}_0(\omega,z)\hat{a}_0(\omega_{p1}+\omega_{p2}-\omega,z)e^{i(\Delta k-\gamma P_1)z} + P_1\hat{a}_0(\omega_{p2},z)\right]. \tag{17}$$

Finally, the evolution of the generated modes' annihilation operators, simplified from Eq. (11), is

$$\frac{\partial\hat{a}_0(\omega,z)}{\partial z} = 2i\gamma[\sqrt{\zeta_2}\sqrt{P_1}\hat{a}_0^\dagger(\omega_{p1}+\omega_{p2}-\omega,z)\hat{a}_0(\omega_{p2},z)e^{-i(\Delta k-\gamma P_1)z} + P_1\hat{a}_0(\omega,z)]. \tag{18}$$

The evolution of both the weak pump and the generated photons can be derived in the low-gain approximation by using a Baker-Hausdorff expansion to first order in the effective gain, $\gamma\sqrt{T\zeta_2}\sqrt{P_1}L \ll 1$. The calculations for the annihilation operators of the generated frequencies are detailed in Appendix B and give the main result

$$\hat{a}_0(\omega,L)e^{-i2\gamma P_1 L} = \hat{a}_0(\omega,0) + 2i\gamma\sqrt{P_1}\sqrt{\zeta_2}Le^{-\frac{iKL}{2}}\mathrm{sinc}\left(\frac{KL}{2}\right)\hat{a}_0^\dagger(\omega_{p1}+\omega_{p2}-\omega,0)\hat{a}_0(\omega_{p2},0),, \tag{19}$$

where $K = \Delta k + \gamma P_1 = \beta(\omega) + \beta(\omega_{p1}+\omega_{p2}-\omega) - \beta(\omega_{p1}) - \beta(\omega_{p2}) + \gamma P_1$ is the total phase mismatch, the sum of the linear and nonlinear parts.

Note that by considering only the first-order gain, we assume that the conversion efficiency is low enough to be well represented by a single conversion process, described by $\hat{a}_0(\omega_{p1},L)\hat{a}_0(\omega_{p2},L)\hat{a}_0^\dagger(\omega,L)\hat{a}_0^\dagger(\omega_{p1}+\omega_{p2}-\omega,L)$. We neglect the reverse process of converting the pairs back to pump photons, which is equivalent to neglecting double-pair emissions in SPDC or standard FWM. This approximation causes deviation of less than 2×10^{-6} for conversion efficiency $\eta = 0.1\%$ and less than 0.02 for a single-photon conversion efficiency up to $\eta = 10\%$, as discussed in Appendix C. A treatment without the low-gain approximation would allow simulation of Rabi oscillations between the single photon and photon pair, as required for the coherent photon conversion of Ref. [14].

III. SINGLE-PHOTON CONVERSION EFFICIENCY

The conversion efficiency of a single photon into a pair can now be derived from Eq. (19). The spectral density of the photons created during the characteristic time T is given by

$$n_{\mathrm{d}}(\omega,L) = \langle\psi|\hat{a}_0^\dagger(\omega,L)\hat{a}_0(\omega,L)|\psi\rangle. \tag{20}$$

The quantum state $|\psi\rangle$ is the input state of the weak pump and generated photon pairs. For a single photon on pump 2, $|\psi\rangle = |1\rangle_{p2}|0\rangle_s|0\rangle_i$, where we label the lower-frequency half of the output pair spectrum *idler* and the higher-frequency half *signal*. The total number of photons generated during T is then given by the integral of the spectral density over the output spectrum.

Putting Eq. (19) into Eq. (20) gives the photon number spectral density per characteristic time

$$n_{\mathrm{d}}(\omega,L) = \frac{T}{2\pi}4\gamma^2 P_1 P_2 L^2 \mathrm{sinc}^2\left(\frac{KL}{2}\right)$$
$$= 4\gamma^2 P_1 \frac{\hbar\omega_{p2}}{2\pi}L^2\mathrm{sinc}^2\left(\frac{KL}{2}\right), \tag{21}$$

where the generation of a photon at frequency ω implies the generation of its pair photon at frequency $\omega_{p1}+\omega_{p2}-\omega$. Let us now find the total number of photon pairs generated out of a single photon in cases of pulsed and continuous-wave pumping.

A. Regime with both pumps pulsed

If both pumps are pulsed simultaneously with a spectral width $\delta\omega_p$ and $T = \frac{2\pi}{\delta\omega_p}$, the total number of photon pairs generated per time T (or per pulse for transform-limited pulses) is

$$N_{\mathrm{pairs/pulse}} = \frac{1}{2}\int d\omega n_{\mathrm{d}}(\omega,L) = 4\gamma^2 P_1 P_2 L^2\frac{\Delta\omega_s}{\delta\omega_p}$$
$$= 4\gamma^2 P_1\frac{\hbar\omega_{p2}}{2\pi}L^2\Delta\omega_s, \tag{22}$$

with

$$\Delta\omega_s = \frac{1}{2}\int d\omega\mathrm{sinc}^2\left(\frac{K(\omega_{p1},\omega_{p2},\omega)L}{2}\right) \tag{23}$$

and $P_2 = \frac{\hbar\omega_{p2}}{T}$, where the factor $1/2$ in the first line is due to the spectrum covering both signal and idler frequencies, leading to double counting. The integral is over the whole spectral range except the two pump frequencies $\omega_{p1,p2}$.

The number of generated photons pairs per second is thus

$$N_{\mathrm{pairs/sec}} = f_{\mathrm{rep}}4\gamma^2 P_1 P_2 L^2\frac{\Delta\omega_s}{\delta\omega_p} = 4\gamma^2 P_{1\mathrm{avg}}P_2 L^2\frac{\Delta\omega_s}{2\pi}, \tag{24}$$

with $P_1 = \frac{P_{1\mathrm{avg}}}{f_{\mathrm{rep}}}\frac{\delta\omega_p}{2\pi}$, where f_{rep} is the repetition rate of the source.

B. Regime with one pump pulsed and the other with a continuous wave

If one of the pumps is pulsed and the other is continuous wave (cw), the output photons will behave as if both pumps were pulsed at the repetition rate of the pulsed one, which removes the necessity for time alignment. Taking the single-photon pump as pulsed and the strong pump as cw, we have $P_1 = P_{1\mathrm{avg}}$ and $P_2 = \frac{\hbar\omega_{p2}}{T}$, which gives

$$N_{\mathrm{pairs/sec}} = f_{\mathrm{rep}}4\gamma^2 P_{1\mathrm{avg}}P_2 L^2\frac{\Delta\omega_s}{\delta\omega_p}. \tag{25}$$

The pair generation is independent of the single-photon pulse duration and depends only on its repetition rate and the strong laser's cw pump power. It is less efficient by a factor of $\frac{f_{\text{rep}}}{\delta\omega_p}$ compared to when both pumps are pulsed.

If we want the weak pump to be cw, we can argue an "equivalent-single-photon" pumping such that each pulse of the strong pump sees, on average, one photon of the weak pump. Then we have to take $P_2 = P_{2\text{avg}} = \frac{\hbar\omega_{p2}}{T}$, and

$$N_{\text{pairs/sec}} = 4\gamma^2 P_{1\text{avg}} P_{2\text{avg}} L^2 \frac{\Delta\omega_s}{2\pi}. \qquad (26)$$

This generation is equivalent to the pulsed-pulsed pumping, which is not surprising since the equivalent-single-photon pumping is cw pumping with the same peak power as the pulsed pumping. This means many more photons of pump p2 enter the fiber, but only the ones which overlap a strong pump pulse can convert into pairs.

C. Regime with two continuous-wave pumps

With an input made out of a weak continuous pump 2 and a strong continuous pump 1, the number of photons generated per second is straightforward,

$$N_{\text{pairs/sec}} = 4\gamma^2 P_{1\text{avg}} P_{2\text{avg}} L^2 \frac{\Delta\omega_s}{2\pi}; \qquad (27)$$

however, it is not obvious to define what qualifies as a single photon for a cw pump. This regime can reach the same efficiency as the pulsed-pulsed case if either of the pumps' cw average power is raised to the peak power of the pulsed-pulsed case. This would be difficult in practice, as peak powers can be four orders of magnitude larger than average powers for the example of mode-locked picosecond lasers.

IV. CANDIDATE FIBERS FOR MAXIMIZING CONVERSION EFFICIENCY

In this section we compare three fiber types with unique methods of phase matching to find the best for single-photon conversion. The single-photon conversion efficiency can be defined, for a weak pumping field composed of N_{p2} photons per time unit, as $\eta = \frac{N_{\text{pairs}}}{N_{p2}}$, with N_{pairs} being the number of photon pairs generated during the same time unit. If the weak pumping field is a single photon, the pulsed-pulsed configuration gives the highest conversion efficiency for a given input average power of pump 1 [compare Eq. (24) with Eqs. (25) and (27)]. Let us consider strategies for maximizing the single-photon conversion in this regime. When $N_{p2} = 1$, the conversion efficiency as given by Eq. (22) is

$$\eta = \frac{N_{\text{pairs}}}{N_{p2}} = 4\gamma^2 P_1 \frac{\hbar\omega_{p2}}{2\pi} L^2 \Delta\omega_s. \qquad (28)$$

The parameters that can be tuned to maximize conversion efficiency are nonlinearity $\chi^{(3)}$ and mode area A_{eff} through γ, length L, phase-matching bandwidth $\Delta\omega_s$, and peak power P_1 of the strong pump. Since γ is squared, decreasing A_{eff} and increasing $\chi^{(3)}$ will have the greatest effect. By contrast, the conversion efficiency appears to be quadratic in the length of the fiber L, but the signal and idler bandwidths given by Eq. (23) will vary approximately with $1/L$, giving an overall

linear dependence on fiber length. The spectral width $\Delta\omega_s$ can also vary independent of L from being tiny ($\delta\omega$) to hundreds of nanometers, depending on the pump configuration and, most importantly, on the type of phase-matching chosen.

We examine three candidates for maximizing conversion efficiency, corresponding to the three main methods of phase matching in optical fibers: birefringence, operation near a zero-dispersion wavelength (ZDW), and nonlinear phase matching using self-phase modulation. The phase-matched frequencies generated by the use of birefringence are spectrally narrow and highly tunable. The frequencies phase matched around the ZDW or due to nonlinear phase modulation can have a broader spectrum and are centered around or near the ZDW. We compare the potential for single-photon conversion in three different fiber types corresponding to those three types of phase matching and find the optimal parameters to maximize pair generation.

The phase mismatch can be expressed as a Taylor expansion around the central frequency ω_0 as

$$\begin{aligned} K(\Omega) &= \beta_2(\omega_0)(\Omega^2 - \Delta\omega^2) \\ &\quad + \frac{\beta_4(\omega_0)}{12}(\Omega^4 - \Delta\omega^4) + \gamma P_1, \end{aligned} \qquad (29)$$

with the central frequency $\omega_0 = \frac{\omega_{p2}+\omega_{p1}}{2}$, the offset frequency $\Omega = \omega - \omega_0$, the pump offset $\Delta\omega = \frac{\omega_{p2}-\omega_{p1}}{2}$, and dispersion coefficients given by

$$\beta_i(\omega_0) = \left(\frac{\partial^i \beta(\omega)}{\partial\omega^i}\right)_{\omega_0}. \qquad (30)$$

Two schemes can be considered when the pump wavelengths are nondegenerate as required for single-photon FWM: external pumping, with generation of new wavelengths in between the pump wavelengths, or internal pumping, with generation of new wavelengths to the exterior. We focus on external pumping as illustrated in Fig. 2 because, assuming the strong pump has the highest wavelength, it allows filtering the main Raman noise from the strong pump as this noise will be at still higher wavelengths. However, the large separation in pump wavelengths can lead to temporal walk-off between the pump pulses in the fiber, reducing efficiency. This effect is mitigated by situating the pumps symmetrically about the ZDW.
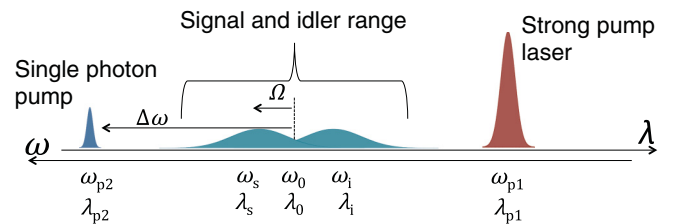
FIG. 2. (Color online) Arrangement of pump and signal-idler wavelengths (amplitudes and widths not to scale). The main source of noise, spontaneous Raman scattering from the strong pump, will occur to the far right of the figure, allowing its removal by spectral filtering.

A. Polarization-maintaining fiber: Birefringent phase matching

A standard polarization-maintaining (PM) fiber exhibits a birefringence large enough to achieve phase matching some dozens to hundreds of terahertz from the pumps ($\sim$100 nm) [22]. These fibers are commercially available, with lengths up to kilometers, and are spatially uniform. The phase matching is easy to obtain and widely tunable by tuning the pump wavelengths. Further, the birefringent phase matching means that the photon pairs can come out from the pumps with opposite polarizations, enabling polarization filtering of the pumps and associated Raman noise. However, the relatively large core size leads to a modest waveguide nonlinear parameter of $\gamma = 4.6 \times 10^{-3}$ W^{-1} m^{-1} in our example below.

We consider the two pumps copolarized along the fast axis and the generated signal and idler polarized along the slow axis, which gives total phase mismatch

$$K(\Omega) = \beta_2(\omega_0)(\Omega^2 - \Delta\omega^2) + \frac{\beta_4(\omega_0)}{12}(\Omega^4 - \Delta\omega^4)$$
$$+ \gamma P_1 + 2\omega_0 \frac{\delta n}{c}, \tag{31}$$

where the birefringence $\delta n = n^{\text{slow}} - n^{\text{fast}}$ is written separately from the dispersion coefficients. Far from the ZDW ($\beta_2 \gg \beta_4, \gamma P_1$), the phase-matched frequencies are

$$\Omega^2 = -\frac{2\omega_0}{\beta_2(\omega_0)} \frac{\delta n}{c} + \Delta\omega^2. \tag{32}$$

We consider a silica PM fiber with birefringence $\delta n = 3 \times 10^{-4}$ (e.g., Panda PM630), and we take both pumps as being pulsed with an 80-MHz repetition rate and 5-ps pulses. We take a 5-W average power for the strong pump and a single photon for the weak pump. With the walk-off length between the two pump pulses in this configuration being 18 cm, we consider an 11-cm fiber, which gives an effective interaction length of $L = 10$ cm.

With the strong pump at 890 nm and the weak pump at 660 nm, we obtain a signal and idler phase matched at 728 and 790 nm with spectral width $\Delta\omega_s = 7$ rad THz (2 nm), as shown in Fig. 3. The conversion efficiency given by Eq. (28) is $\eta = 2 \times 10^{-8}$, well below that achievable in $\chi^{(2)}$ media. We plot the signal and idler spectral density [photons per (rad Hz) per pulse] in Fig. 3, accurate to the precision of our frequency-space mapping, $\delta\omega_p = 1.3$ rad THz (0.5 nm, given by the width of the gray lines on the graph).

B. Microstructured fiber: Phase matching near the zero-dispersion wavelength

Phase matching occurs in a fiber near the ZDW when the material and waveguide contributions to dispersion cancel. We will take the example of silica microstructured fibers, which are commercially available and can be fabricated to exhibit a ZDW in the visible and telecom ranges. The interest in such a fiber is that the core can be much smaller than regular single-mode fibers, thus increasing the waveguide nonlinear parameter, e.g., up to $\gamma = 2.7 \times 10^{-2}$ W^{-1} m^{-1} in our example, with lengths up to a few meters [23]. The spectral broadness of the phase matching depends on the length considered and is only tunable in a small range once the ZDW is chosen.
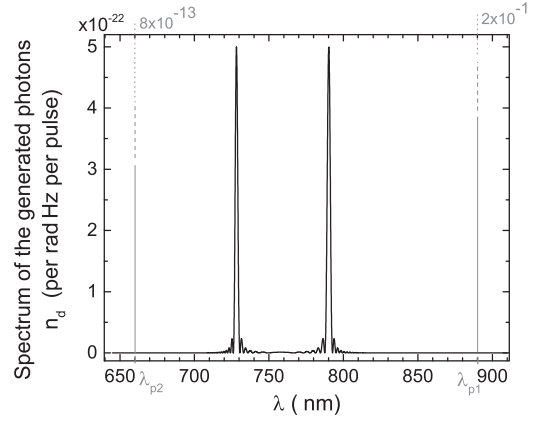
FIG. 3. Converting a single photon to a pair via FWM is possible in principle using a PM fiber, but the very narrow phase matching limits the efficiency to $\eta = 2 \times 10^{-8}$ in this example. The quasimonochromatic pump wavelengths are represented by gray lines with a width of 1.3 rad THz with values labeled above the graph (well above the y axis shown), while the generated signal and idler spectra are the black lines in the center.

We model a microstructured fiber with a core diameter of 1.8 μm and air fraction of 0.72 in the cladding, which give the ZDW at 716 nm. The wavelengths and the pump powers are altered slightly from the previous example to achieve phase matching. We take a 1-W average power for the strong pump in a 2-m-long fiber, with 2-ps-long pump pulses and 2-ps-long single-photon pulses at an 80-MHz repetition rate. As a consequence of working near the ZDW, the walk-off length is now over 100 m since the pumps have approximately the same propagation constant β on either side of the ZDW. The single-photon frequency is at a wavelength of 676.75 nm, and the strong pump is now at 760 nm. Simulations give a much broader spectrum for the signal and idler (around 160 rad THz; Fig. 4), and consequently, the efficiency, still given by Eq. (28),
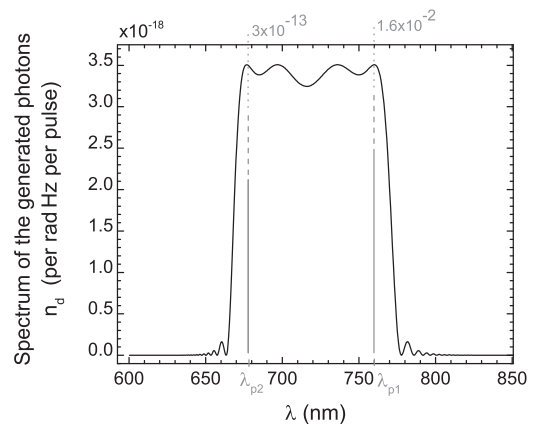
FIG. 4. A much broader signal and idler spectrum is obtained near the ZDW using a microstructured fiber. Even after filtering between 686 and 750 nm to remove noise photons near the pumps, the efficiency $\eta = 4 \times 10^{-4}$ over the remaining signal-idler range is four orders of magnitude larger than for the PM fiber. The gray lines represent the pumps' wavelengths, widths (now 3.1 rad THz), and intensity as in Fig. 3.

is now up to $\eta = 4 \times 10^{-4}$. Even including filtration of the generated photons between 686 and 750 nm to allow pump removal, this efficiency is four orders of magnitude better than the PM fiber.

However, this method of phase matching is very sensitive to core diameter and pump wavelengths. For example, a 0.5-nm deviation of pump wavelength changes the output spectral shape completely and, even if it is still phase matched, may give no pairs at the center of the spectrum. Additionally, obtaining a 2-m microstructured fiber with good uniformity for the whole length is not straightforward, as some variations in the core diameter will occur that deteriorate the perfect phase matching.

C. Chalcogenide microwire fiber: Phase matching due to self-phase modulation

Achieving the best conversion efficiency requires ultrahigh nonlinearity and small cross-sectional area. These can be achieved by tapering fibers made of chalcogenide glass as in Refs. [24,25]. The chalcogenide As_2Se_3 has $\chi^{(3)}$ three orders of magnitude larger than that of silica glass, and core diameters in the tapered microwire region can be as small as 500 nm, thanks to its large refractive index, while still maintaining good coupling to standard single-mode fibers and lengths beyond 10 cm. These microwires exhibit ultrahigh waveguide nonlinear parameters up to $\gamma = 180\ \mathrm{W}^{-1}\ \mathrm{m}^{-1}$.

This large γ directly leads to high conversion efficiency but also allows nonlinear phase matching. As shown by Eq. (29), it is possible to compensate for positive or negative linear phase mismatch by the nonlinear contribution γP_1 due to the strong-pump self-phase modulation. The higher the dispersive mismatch is, the higher the pump powers must be to compensate, so moderate pump powers still require working near the ZDW. In the external-pumping configuration of Fig. 2, the dispersion β_2 or β_4 has to be positive to compensate for self-phase modulation because the pump offset is greater than the frequency offset, i.e., $\Delta\omega^2 > \Omega^2$. The pump power necessary to reach perfect phase matching is

$$P_1 = \frac{1}{\gamma}\left(\beta_2(\omega_0)\Delta\omega^2 + \frac{\beta_4(\omega_0)}{12}\Delta\omega^4\right). \qquad (33)$$

For convenient all-telecom operation and to avoid the two-photon absorption at short wavelengths in the chalcogenide glass As_2Se_3 [26], we take the example of the FWM scheme pumped at 1480 nm by the single photon and at 1620 nm by a strong pump. The two fields are pulsed at 80 MHz with 2-ps-long pulses. The fiber considered is similar to the samples described in Ref. [25]. A fiber diameter of $0.555\ \mu m$ for the microwire gives a dispersion coefficient of $\beta_2(\omega_0) = 0.05\ \mathrm{ps}^2/\mathrm{m}$ at 1550 nm, and β_4 is negligible. Phase matching is achieved for a 0.8-W peak power, which corresponds to an average power of only 0.13 mW. Simulation of the spectral density is given in Fig. 5 in a 10-cm-long microwire section, where the walk-off length between the two pump pulses is now so large that it is effectively infinite. Both the high intrinsic $\chi^{(3)}$ of the chalcogenide and the strong confinement allow us to reach a conversion efficiency of $\eta = 1.1 \times 10^{-3}$. However, as in the silica microstructured fibers, caution must be taken in filtering the desired photons since high nonlinearity means high Raman noise, large phase modulation broadening, and
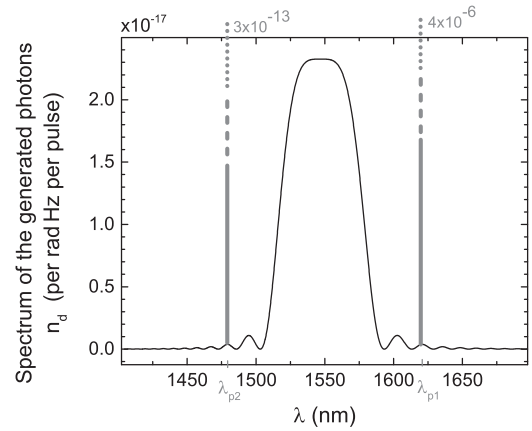
FIG. 5. Due to high intrinsic $\chi^{(3)}$ and strong confinement, the chalcogenide microwire gives the highest conversion rate, with an efficiency of $\eta = 1.1 \times 10^{-3}$. The gray lines represent the pumps' wavelengths, widths (3.1 rad THz), and intensity, as in Fig. 3.

other undesired interactions such as degenerate FWM from the strong pump.

D. Experiments

Tests in our laboratory have shown that the nonlinear interaction in standard birefringent fibers is indeed very weak, making them unsuitable for single-photon conversion. The implementation in Ref. [14] in birefringent microstructured fibers allowed an inferred conversion efficiency of 3×10^{-9}, with the weak pump kept at $4.8\text{-}\mu\mathrm{W}$ effective average power, well above the single-photon level. This was achieved for strong-pump average powers under 100 mW and employed narrow-band birefringent phase matching, limiting conversion efficiency but demonstrating the principle of single-photon conversion. Finally, we have performed preliminary experiments on the chalcogenide microwires, verifying nondegenerate, external-pumping phase-matching conditions similar to those shown above.

V. CONCLUSION

We have predicted a promising result in the conversion of single photons into pairs via four-wave mixing. As shown from our simulations based on the evolution of the quantum field operators, conversion efficiencies up to 0.1% should be achievable in chalcogenide microwires. The results in the three types of fibers we modeled are summarized in Table I.

In this work, the low-gain approximation is sufficient for applications to generate large entangled states and photon heralding, although a nonperturbative approach keeping all orders of gain would make for an interesting study and would allow exploring the deterministic pair generation $|1\rangle_{p2} \rightarrow |11\rangle_{si}$ and oscillatory $|1\rangle_{p2} \rightarrow |11\rangle_{si} \rightarrow |1\rangle_{p2} \rightarrow \cdots$ regimes. However, finding a material enabling photon conversion with an efficiency high enough to justify this nonperturbative approach remains a challenge.

Interestingly, neither the derivation nor the value of the conversion efficiency we found depends on the single photon being quantized: the result can equally be obtained by

TABLE I. Summary of expected single-photon-to-pair conversion efficiency and strong-pump power required for the three fiber types considered: birefringent silica fibers, microstructured silica fibers, and chalcogenide As_2Se_3 microwired fibers. Considering the 80-MHz repetition rate and inputting one photon per pulse, we also calculate the number of pairs produced per second.

Fiber type	Average pump power (mW)	Conversion efficiency η	Photon pairs per second
Birefringent (silica)	5000	2×10^{-8}	1.6
Microstructured (silica)	1000	4×10^{-4}	32 000
Microwire (As_2Se_3)	0.13	1×10^{-3}	80 000

assuming a classical pulse with the same input peak power as the single photon. This implies there is no new quantumness in this process beyond the well-established spontaneous generation of pairs in standard spontaneous FWM or SPDC.

In implementations, attention must be paid to the various possible sources of noise: degenerate FWM and spontaneous Raman scattering [27] from the strong pump and even second orders or combinations of these effects.

APPENDIX A: DERIVATION OF MOMENTUM GENERATORS

The two pumps are considered to be monochromatic or quasimonochromatic and perfectly overlapping, with identical pulse duration and spectral width $\delta\omega$. The quantization time is chosen to be the transform-limited pulse duration, $T = 2\pi/\delta\omega$.

The quantum field operator can be written in the continuous limit as

$$\hat{E}(z,t) = \int d\omega \sqrt{\Omega(\omega)} \hat{a}(\omega,z) e^{-i\omega t} + \text{H.c.}, \quad \text{(A1)}$$

where the integral runs from zero to infinity, with the notation simplified by the introduction of the variable $\Omega(\omega) = \frac{\hbar\omega}{4\pi\varepsilon_0 c A_{\text{eff}} n(\omega)}$.

The momentum operator is given by Eq. (4), from which we can derive its linear part $\hat{G}_l(z)$ and nonlinear part $\hat{G}_{nl}(z)$.

$$\hat{G}_l(z) = \int_{A_{\text{eff}}} dS \int_0^{+T} dt \iint d\omega d\omega' \varepsilon_0 [\chi^{(1)}(\omega) + 1]$$
$$\times \sqrt{\Omega(\omega)} \hat{a}^\dagger(\omega,z) e^{i\omega t} \sqrt{\Omega(\omega')} \hat{a}(\omega',z) e^{-i\omega' t} + \text{H.c.}$$
$$= 2A_{\text{eff}} \iint d\omega d\omega' \varepsilon_0 n(\omega)^2 \Omega(\omega) \hat{a}^\dagger(\omega,z) \hat{a}(\omega,z)$$
$$\times 2\pi \delta(\omega - \omega')$$
$$= 4\pi A_{\text{eff}} \varepsilon_0 \int d\omega n(\omega)^2 \Omega(\omega) \hat{a}^\dagger(\omega,z) \hat{a}(\omega,z)$$
$$= \int d\omega \frac{\hbar\omega}{c} n(\omega) \hat{a}^\dagger(\omega,z) \hat{a}(\omega,z),$$

where we used $\int_0^T dt e^{i(\omega-\omega')t} = 2\pi\delta(\omega - \omega')$ (since the integration time matches the quantization time). The linear evolution of any annihilation operator can thus be deduced as in Eq. (7). The nonlinear momentum operator evolves according to

$$\hat{G}_{nl}(z) = \int_{A_{\text{eff}}} dS \int_0^{+T} dt \hat{P}_{nl}^{(-)}(z,t) \hat{E}^{(+)}(z,t) + \text{H.c.} \quad \text{(A2)}$$

If we consider only FWM as generating propagating modes, the relevant nonlinear polarization is $\hat{P}_{nl}(z,t) = \varepsilon_0 \chi^{(3)} \vdots \hat{E}^3(z,t)$. We can decompose $\hat{G}_{nl}(z)$ into two parts, one for FWM and the other for phase modulation, as $\hat{G}_{nl}(z) = \hat{G}_{nl}^{\text{FWM}}(z) + \hat{G}_{nl}^{\text{phMod}}(z)$. Then

$$\hat{G}_{nl}(z) = \varepsilon_0 \chi^{(3)} \int_{A_{\text{eff}}} dS \int_0^{+T} dt$$
$$\times \left[\int d\omega \sqrt{\Omega(\omega)} \hat{a}^\dagger(\omega,z) e^{i\omega t} + \text{H.c.} \right]$$
$$\times \left[\int d\omega' \sqrt{\Omega(\omega')} \hat{a}^\dagger(\omega',z) e^{i\omega' t} + \text{H.c.} \right]$$
$$\times \left[\int d\omega'' \sqrt{\Omega(\omega'')} \hat{a}^\dagger(\omega'',z) e^{i\omega'' t} + \text{H.c.} \right]$$
$$\times \left[\int d\omega''' \sqrt{\Omega(\omega''')} \hat{a}^\dagger(\omega''',z) e^{i\omega''' t} + \text{H.c.} \right]. \quad \text{(A3)}$$

We keep only the frequencies that will propagate in the fiber: the frequencies around the two pumps and frequencies generated by FWM with these two pumps. We can separate the operators into four frequency parts,

$$\int d\omega \sqrt{\Omega(\omega)} \hat{a}(\omega,z) e^{-i\omega t} = \int_{\Delta\omega_{p1}} d\omega_1 \sqrt{\Omega(\omega_1)} \hat{a}(\omega_1,z) e^{-i\omega_1 t} + \int_{\Delta\omega_{p2}} d\omega_2 \sqrt{\Omega(\omega_2)} \hat{a}(\omega_2,z) e^{-i\omega_2 t}$$
$$+ \int_{\Delta\omega_s} d\omega \sqrt{\Omega(\omega)} \hat{a}(\omega,z) e^{-i\omega t} + \int_{\Delta\omega_i} d\omega' \sqrt{\Omega(\omega')} \hat{a}(\omega',z) e^{-i\omega' t}, \quad \text{(A4)}$$

where $\Delta\omega_s$ and $\Delta\omega_i$ are a wide frequency range around the central frequencies of the photon pairs generated by FWM and $\Delta\omega_{p1,p2}$ are a wide range frequency around the two pump wavelengths. Since we assumed our two pumps are monochromatic or quasimonochromatic and took their bandwidth to be the frequency step $\Delta\omega_{p1} = \Delta\omega_{p2} = \delta\omega = 2\pi/T$, we can write $\int_{\Delta\omega_{p1}} d\omega_1 \sqrt{\Omega(\omega_1)} \hat{a}(\omega_1,z) = \delta\omega \sqrt{\Omega(\omega_{p1})} \hat{a}(\omega_{p1},z) = \frac{2\pi}{T} \sqrt{\Omega(\omega_{p1})} \hat{a}(\omega_{p1},z)$, with ω_{p1} being the central frequency of pump 1, and we can do the same for pump 2. For more clarity in the expressions with respect to the other operators, we keep the pump

mode operators dimensioned as $[\hat{a}(\omega_{p1,p2},z)] = \sqrt{\frac{1}{\delta\omega}}$, so the number of pump photons traveling through a plane of position z during the time interval T is $\frac{2\pi}{T}\langle\hat{a}^{\dagger}(\omega_{p1,2},z)\hat{a}(\omega_{p1,2},z)\rangle$. Then we can write

$$\int d\omega \sqrt{\Omega(\omega)}\hat{a}(\omega,z)e^{-i\omega t} = \frac{2\pi}{T}[\sqrt{\Omega(\omega_{p1})}\hat{a}(\omega_{p1},z)e^{-i\omega_{p1}t} + \sqrt{\Omega(\omega_{p2})}\hat{a}(\omega_{p2},z)e^{-i\omega_{p2}t}]$$

$$+ \int_{\Delta\omega_s} d\omega \sqrt{\Omega(\omega)}\hat{a}(\omega,z)e^{-i\omega t} + \int_{\Delta\omega_i} d\omega' \sqrt{\Omega(\omega')}\hat{a}(\omega',z)e^{-i\omega' t}. \tag{A5}$$

The FWM part of the nonlinear momentum is then

$$\hat{G}_{nl}^{\text{FWM}}(z) = 24\left(\frac{2\pi}{T}\right)^2 \varepsilon_0\chi^{(3)} \int_{A_{\text{eff}}} dS \int_0^{+T} dt \int_{\Delta\omega_s} d\omega \sqrt{\Omega(\omega)}\hat{a}^{\dagger}(\omega,z)$$

$$\times \int_{\Delta\omega_i} d\omega' \sqrt{\Omega(\omega')}\hat{a}^{\dagger}(\omega',z)\sqrt{\Omega(\omega_{p1})}\hat{a}(\omega_{p1},z)\sqrt{\Omega(\omega_{p2})}\hat{a}(\omega_{p2},z)e^{i\Delta\omega t} + \text{H.c.},$$

or, if we write the operators as a product of their linear and nonlinear parts,

$$\hat{G}_{nl}^{\text{FWM}}(z) = 24\left(\frac{2\pi}{T}\right)^2 \varepsilon_0\chi^{(3)} \int_{A_{\text{eff}}} dS \int_0^{+T} dt \int_{\Delta\omega_s} d\omega \sqrt{\Omega(\omega)}\hat{a}_0^{\dagger}(\omega,z)$$

$$\times \int_{\Delta\omega_i} d\omega' \sqrt{\Omega(\omega')}\hat{a}_0^{\dagger}(\omega',z)\sqrt{\Omega(\omega_{p1})}\hat{a}_0(\omega_{p1},z)\sqrt{\Omega(\omega_{p2})}\hat{a}_0(\omega_{p2},z)e^{i\Delta\omega t}e^{-i\Delta k z} + \text{H.c.}$$

The factor of 24 comes from all the possible combinations of the mode operators. Here $\Delta\omega = \omega + \omega' - \omega_{p1} - \omega_{p2}$ and $\Delta k = \beta(\omega) + \beta(\omega') - \beta(\omega_{p1}) - \beta(\omega_{p2})$. Using again $\int_0^T dt e^{i\Delta\omega t} = 2\pi\delta(\Delta\omega)$ and $\int d\omega'\delta(\Delta\omega) = 1$ and evaluating the cross-sectional area integral, we have

$$\hat{G}_{nl}^{\text{FWM}}(z) = 24 \times 2\pi \left(\frac{2\pi}{T}\right)^2 \varepsilon_0\chi^{(3)} A_{\text{eff}} \sqrt{\Omega(\omega_{p1})}\sqrt{\Omega(\omega_{p2})} \int_{\Delta\omega_s} d\omega \sqrt{\Omega(\omega)}\sqrt{\Omega(\omega_{p1} + \omega_{p2} - \omega)}$$

$$\times \hat{a}_0^{\dagger}(\omega,z)\hat{a}_0^{\dagger}(\omega_{p1} + \omega_{p2} - \omega,z)\hat{a}_0(\omega_{p1},z)\hat{a}_0(\omega_{p2},z)e^{-i\Delta k z} + \text{H.c.} \tag{A6}$$

We can extend the integral over the signal over the whole spectrum except for the two pumps' frequencies and add a factor of $1/2$ for double-counting signal and idler frequencies. Then

$$\hat{G}_{nl}^{\text{FWM}}(z) = 3\frac{2\pi}{T}\chi^{(3)}\frac{\hbar^2}{\varepsilon_0 c^2 A_{\text{eff}} T}\sqrt{\frac{\omega_{p1}}{n(\omega_{p1})}\frac{\omega_{p2}}{n(\omega_{p2})}} \int d\omega \sqrt{\frac{\omega}{n(\omega)}}\sqrt{\frac{\omega_{p1} + \omega_{p2} - \omega}{n(\omega_{p1} + \omega_{p2} - \omega)}}\hat{a}_0^{\dagger}(\omega,z)$$

$$\times \hat{a}_0^{\dagger}(\omega_{p1} + \omega_{p2} - \omega,z)\hat{a}_0(\omega_{p1},z)\hat{a}_0(\omega_{p2},z)e^{-i\Delta k z} + \text{H.c.} \tag{A7}$$

Now let's look for the phase modulation term. By definition of phase modulation, we keep only the terms with no phase that arise from the expansion of the nonlinear momentum, (A3). We then obtain

$$\hat{G}_{nl}^{\text{ph mod}}(z) = \int_{A_{\text{eff}}} dS \varepsilon_0\chi^{(3)} \Bigg[6\left(\frac{2\pi}{T}\right) \sum_{k=s,i,p_1,p_2} \left(\int_{\Delta\omega_k} d\omega \Omega(\omega)\hat{a}_0^{\dagger}(\omega,z)\hat{a}_0(\omega,z)\right)^2$$

$$+ 12\left(\frac{2\pi}{T}\right) \sum_{k=s,i,p_1,p_2} \sum_{j\neq k} \left(\frac{2\pi}{T}\right) \int_{\Delta\omega_k} d\omega \int_{\Delta\omega_j} d\omega' \Omega(\omega)\Omega(\omega')\hat{a}_0^{\dagger}(\omega,z)\hat{a}_0(\omega,z)\hat{a}_0^{\dagger}(\omega',z)\hat{a}_0(\omega',z) \Bigg], \tag{A8}$$

and if we sum over all the frequencies in the integrals, the momentum generator collapses into

$$\hat{G}_{nl}^{\text{ph mod}}(z) = \left(\frac{2\pi}{T}\right) 2\pi A_{\text{eff}} \varepsilon_0\chi^{(3)} \Bigg\{ 12 \iint d\omega d\omega' \Omega(\omega)\Omega(\omega')\hat{a}_0^{\dagger}(\omega,z)\hat{a}_0(\omega',z)\hat{a}_0^{\dagger}(\omega',z)\hat{a}_0(\omega,z)$$

$$- 6\int d\omega \frac{2\pi}{T}[\Omega(\omega)\hat{a}_0^{\dagger}(\omega,z)\hat{a}_0(\omega,z)]^2 \Bigg\}, \tag{A9}$$

or

$$\hat{G}_{nl}^{\text{ph mod}}(z) = 3\chi^{(3)}\frac{\hbar^2}{\varepsilon_0 c^2 A_{\text{eff}} T} \Bigg[\iint d\omega d\omega' \frac{\omega}{n(\omega)}\frac{\omega'}{n(\omega')}\hat{a}_0^{\dagger}(\omega,z)\hat{a}_0(\omega',z)\hat{a}_0^{\dagger}(\omega',z)\hat{a}_0(\omega,z)$$

$$- \frac{1}{2}\int d\omega \frac{2\pi}{T}\left(\frac{\omega}{n(\omega)}\hat{a}_0^{\dagger}(\omega,z)\hat{a}_0(\omega,z)\right)^2 \Bigg]. \tag{A10}$$

APPENDIX B: LOW-GAIN APPROXIMATION AND DERIVATION OF MODE OPERATORS

We can now derive the mode operators from Eq. (3) for any frequency generated in the fiber, which gives Eqs. (10)–(12).

We proceed by first factoring out the phase modulation with the variable change $\hat{a}_0(\omega,z) = \hat{a}'_0(\omega,z)e^{i2\gamma P_1 z}$, which gives, for the generated modes' FWM evolution,

$$\frac{\partial \hat{a}'_0(\omega,z)}{\partial z}e^{i2\gamma P_1 z} + i2\gamma P_1 \hat{a}'_0(\omega,z)e^{i2\gamma P_1 z} = 2i\gamma\sqrt{P_1}\sqrt{\zeta_2}\hat{a}'^\dagger_0(\omega_{p1}+\omega_{p2}-\omega,z)\hat{a}'_0(\omega_{p2},z)e^{-i(\Delta k - \gamma P_1)z} + 2i\gamma P_1 \hat{a}'_0(\omega,z)e^{i2\gamma P_1 z},$$

(B1)

so

$$\frac{\partial \hat{a}'_0(\omega,z)}{\partial z} = 2i\gamma\sqrt{P_1}\sqrt{\zeta_2}\hat{a}'^\dagger_0(\omega_{p1}+\omega_{p2}-\omega,z)\hat{a}'_0(\omega_{p2},z)e^{-i(\Delta k+\gamma P_1)z}.$$

(B2)

For the weak pump it gives

$$\frac{\partial \hat{a}'_0(\omega_{p2},z)}{\partial z}e^{i2\gamma P_1 z} + i2\gamma P_1 \hat{a}'_0(\omega_{p2},z)e^{i2\gamma P_1 z} = 2i\gamma P_1 \hat{a}'_0(\omega_{p2},z)e^{i2\gamma P_1 z} + 2i\gamma\sqrt{P_1}\sqrt{\zeta_2}\frac{T}{2\pi}$$

$$\times \int d\omega \sqrt{\frac{\omega(\omega_{p1}+\omega_{p2}-\omega)}{\omega_{p1}\omega_{p2}}}\hat{a}'_0(\omega,z)\hat{a}'_0(\omega_{p1}+\omega_{p2}-\omega,z)e^{i(\Delta k+\gamma P_1)z},$$

(B3)

or

$$\frac{\partial \hat{a}'_0(\omega_{p2},z)}{\partial z} = 2i\gamma\sqrt{P_1}\sqrt{\zeta_2}\frac{T}{2\pi}\int d\omega \sqrt{\frac{\omega(\omega_{p1}+\omega_{p2}-\omega)}{\omega_{p1}\omega_{p2}}}\hat{a}'_0(\omega,z)\hat{a}'_0(\omega_{p1}+\omega_{p2}-\omega,z)e^{i(\Delta k+\gamma P_1)z}.$$

(B4)

The total phase mismatch is now $K = \Delta k + \gamma P_1$. The modes' evolution can be solved by performing a Baker-Hausdorff expansion. If the z evolution of the momentum operator $\hat{G}(z)$ is slow enough to be considered to be z independent, which is the case in a low-gain interaction, $\int_0^L \hat{G}_{nl}(z)dz \simeq \hat{G}_{nl}L$ and $\hat{a}_0(\omega,L) = e^{-\frac{i}{\hbar}\hat{G}_{nl}L}\hat{a}_0(\omega,0)e^{+\frac{i}{\hbar}\hat{G}_{nl}L}$, which gives

$$\hat{a}_0(\omega,L) = \hat{a}_0(\omega,0) + \left[\hat{a}_0(\omega,0),\frac{i}{\hbar}\hat{G}_{nl}L\right] + \frac{1}{2!}\left[\left[\hat{a}_0(\omega,0),\frac{i}{\hbar}\hat{G}_{nl}L\right],\frac{i}{\hbar}\hat{G}_{nl}L\right]$$

$$+ \frac{1}{3!}\left[\left[\left[\hat{a}_0(\omega,0),\frac{i}{\hbar}\hat{G}_{nl}L\right],\frac{i}{\hbar}\hat{G}_{nl}L\right],\frac{i}{\hbar}\hat{G}_{nl}L\right] + \cdots,$$

(B5)

or, given that $\frac{i}{\hbar}[\hat{a}_0(\omega,0),\hat{G}_{nl}(L)] = (\frac{\partial \hat{a}_0(\omega,z)}{\partial z})_{z=0}$,

$$\hat{a}_0(\omega,L) = \hat{a}_0(\omega,0) + \left(\frac{\partial \hat{a}_0(\omega,z)}{\partial z}\right)_{z=0}L + \left(\frac{\partial^2 \hat{a}_0(\omega,z)}{\partial z^2}\right)_{z=0}\frac{L^2}{2!} + \left(\frac{\partial^3 \hat{a}_0(\omega,z)}{\partial z^3}\right)_{z=0}\frac{L^3}{3!} + \cdots.$$

(B6)

Development (B6), equivalent to a Taylor expansion for the operators, gives the creation and annihilation operators at the output of the medium for the generated modes and the weak pump, solutions of Eqs. (B2) and (B4), respectively. Let's solve (B7) for the generated modes.

Equation (B2) gives, for the higher-order derivatives,

$$\frac{\partial^2 \hat{a}'_0(\omega,z)}{\partial z^2} = -iK2i\gamma\sqrt{P_1}\sqrt{\zeta_2}\hat{a}'^\dagger_0(\omega_{p1}+\omega_{p2}-\omega,z)\hat{a}'_0(\omega_{p2},z)e^{-iKz} + 2i\gamma\sqrt{P_1}\sqrt{\zeta_2}\frac{\partial \hat{a}'^\dagger_0(\omega_{p1}+\omega_{p2}-\omega,z)}{\partial z}\hat{a}'_0(\omega_{p2},z)e^{-iKz}$$

$$+ 2i\gamma\sqrt{P_1}\sqrt{\zeta_2}\hat{a}'^\dagger_0(\omega_{p1}+\omega_{p2}-\omega,z)\frac{\partial \hat{a}'_0(\omega_{p2},z)}{\partial z}e^{-iKz},$$

(B7)

so

$$\frac{\partial^2 \hat{a}'_0(\omega,z)}{\partial z^2} = -iK2i\gamma\sqrt{P_1}\sqrt{\zeta_2}\hat{a}'^\dagger_0(\omega_{p1}+\omega_{p2}-\omega,z)\hat{a}'_0(\omega_{p2},z)e^{-iKz} + (2i\gamma\sqrt{P_1}\sqrt{\zeta_2})^2\hat{a}'^\dagger_0(\omega,z)\hat{a}'_0(\omega_{p2},z)\hat{a}'_0(\omega_{p2},z)e^{-iKz}e^{iKz}$$

$$+ (2i\gamma\sqrt{P_1}\sqrt{\zeta_2})^2\frac{T}{2\pi}\int d\omega \sqrt{\frac{\omega(\omega_{p1}+\omega_{p2}-\omega)}{\omega_{p1}\omega_{p2}}}\hat{a}'^\dagger_0(\omega_{p1}+\omega_{p2}-\omega,z)\hat{a}'_0(\omega,z)\hat{a}'_0(\omega_{p1}+\omega_{p2}-\omega,z)e^{-iKz}e^{-iKz}.$$

(B8)

Since the quantity $\gamma\sqrt{P_1}\sqrt{\frac{T}{2\pi}\zeta_2}$ is very small [it is the square-root number of photons generated in 1 m of medium within a frequency range of $\delta\omega$; see the link to the efficiency η in Eq. (28)], we will limit our development to the first order in $\gamma\sqrt{P_1}\sqrt{\frac{T}{2\pi}\zeta_2}$. This approximation is physically equivalent to neglecting all the phenomena involving more than a single pair

creation, in particular here the recombination of a created pair back into pump photons and the Rabi oscillations that can then occur between signal-idler and pump photon states. Then we have

$$\frac{\partial^2 \hat{a}'_0(\omega,z)}{\partial z^2} = -iK2i\gamma\sqrt{P_1}\sqrt{\zeta_2}\hat{a}'^\dagger_0(\omega_{p1}+\omega_{p2}-\omega,z)\hat{a}'_0(\omega_{p2},z)e^{-iKz}. \tag{B9}$$

By doing the same approximation for the third order we get

$$\frac{\partial^3 \hat{a}'_0(\omega,z)}{\partial z^3} = (-iK)^2 2i\gamma\sqrt{P_1}\sqrt{\zeta_2}\hat{a}'^\dagger_0(\omega_{p1}+\omega_{p2}-\omega,z)\hat{a}'_0(\omega_{p2},z)e^{-iKz}, \tag{B10}$$

and by an obvious recurrence

$$\frac{\partial^n \hat{a}'_0(\omega,z)}{\partial z^n} = (-iK)^{n-1} 2i\gamma\sqrt{P_1}\sqrt{\zeta_2}\hat{a}'_0(\omega_{p1}+\omega_{p2}-\omega,z)\hat{a}'^+_0(\omega_{p2},z)e^{-iKz}. \tag{B11}$$

Then Eq. (B6) gives

$$\hat{a}'_0(\omega,L) = \hat{a}'_0(\omega,0) + 2i\gamma\sqrt{P_1}\sqrt{\zeta_2}\hat{a}'^\dagger_0(\omega_{p1}+\omega_{p2}-\omega,0)\hat{a}'_0(\omega_{p2},0)e^{-iKL}\sum_{n=1}^{+\infty}\frac{L^n}{n!}(-iK)^{n-1}.$$

The power series can be simplified to

$$\sum_{n=1}^{+\infty}\frac{L^n}{n!}(-iK)^{n-1} = L\sum_{n=1}^{+\infty}\frac{(-iKL)^{n-1}}{n!} = L\frac{e^{-iKL}-1}{-iKL} = e^{-\frac{iKL}{2}}L\,\mathrm{sinc}\left(\frac{KL}{2}\right), \tag{B12}$$

so

$$\hat{a}'_0(\omega,L) = \hat{a}'_0(\omega,0) + 2i\gamma\sqrt{P_1}\sqrt{\zeta_2}e^{-\frac{iKL}{2}}L\,\mathrm{sinc}\left(\frac{KL}{2}\right)\hat{a}'^\dagger_0(\omega_{p1}+\omega_{p2}-\omega,0)\hat{a}'_0(\omega_{p2},0).$$

Then with $\hat{a}_0(\omega,z) = \hat{a}'_0(\omega,z)e^{i2\gamma P_1 z}$,

$$\hat{a}_0(\omega,L)e^{-i2\gamma P_1 L} = \hat{a}_0(\omega,0) + 2i\gamma\sqrt{P_1}\sqrt{\zeta_2}e^{-\frac{iKL}{2}}L\,\mathrm{sinc}\left(\frac{KL}{2}\right)\hat{a}_0^\dagger(\omega_{p1}+\omega_{p2}-\omega,0)\hat{a}_0(\omega_{p2},0).$$

APPENDIX C: VALIDITY OF LOW-GAIN APPROXIMATION

In Appendix B we developed the creation- and annihilation-operator evolution to the first order in the gain. If η, as defined in Eq. (28), is much less than 1, it is the efficiency of conversion of a single photon into a pair. Searching for the precision of this result, we have to go to higher orders in gain in the development of Appendix B. Going to the second order in η allows the possibility of having a pair converted back into a single photon, which occurs with probability η^2, but the forward single-photon conversion efficiency is unchanged. Going to the third order in η then lowers the single-photon conversion efficiency to $\eta - 2\eta^2 + \eta^3$. This result allows us to define the error due to taking the gain to first order as $2\eta^2$.

In principle, η could have an arbitrarily large value by increasing the strong-pump power. When η approaches and goes beyond 1, it cannot be defined as a probability of conversion, and we must solve exactly the operator evolution. As developed in a classical setting in Ref. [28], elliptic functions are expected for the beams' intensity evolution, giving Rabi-like oscillations between the pump photon and the signal-idler pair state. As noted in Ref. [14], the higher η is, the more oscillations will occur in the fiber, but this is again a theoretical scheme taking only nondegenerate FWM into account. Parasitic phenomena, in particular self-phase modulation, will also become ultrahigh in this regime.

[1] D. C. Burnham and D. L. Weinberg, Phys. Rev. Lett. **25**, 84 (1970).

[2] M. Fiorentino, P. Voss, J. Sharping, and P. Kumar, IEEE Photonics Technol. Lett. **14**, 983 (2002).

[3] T. Guerreiro, E. Pomarico, B. Sanguinetti, N. Sangouard, J. S. Pelc, C. Langrock, M. M. Fejer, H. Zbinden, R. T. Thew, and N. Gisin, Nat. Commun. **4**, 2324 (2013).

[4] D. R. Hamel, L. K. Shalm, H. Hübel, A. J. Miller, F. Marsili, V. B. Verma, R. P. Mirin, S. W. Nam, K. J. Resch, and T. Jennewein, Nat. Photon. **8**, 801 (2014).

[5] Y. Miwa, J.-i. Yoshikawa, N. Iwata, M. Endo, P. Marek, R. Filip, P. van Loock, and A. Furusawa, Phys. Rev. Lett. **113**, 013601 (2014).

[6] H. Huebel, D. R. Hamel, A. Fedrizzi, S. Ramelow, K. J. Resch, and T. Jennewein, Nature (London) **466**, 601 (2010).

[7] L. K. Shalm, D. R. Hamel, Z. Yan, C. Simon, K. J. Resch, and T. Jennewein, Nat. Phys. **9**, 19 (2013).

[8] D. E. Browne and T. Rudolph, Phys. Rev. Lett. **95**, 010501 (2005).

[9] M. Hillery, V. Buzek, and A. Berthiaume, Phys. Rev. A **59**, 1829 (1999).

[10] K. Banaszek and P. L. Knight, Phys. Rev. A **55**, 2368 (1997).

[11] D. M. Greenberger, M. A. Horne, A. Shimony, and A. Zeilinger, Am. J. Phys. **58**, 1131 (1990).

[12] A. Cabello and F. Sciarrino, Phys. Rev. X **2**, 021010 (2012).

[13] N. Gisin, S. Pironio, and N. Sangouard, Phys. Rev. Lett. **105**, 070501 (2010).

[14] N. K. Langford, S. Ramelow, R. Prevedel, W. J. Munro, G. J. Milburn, and A. Zeilinger, Nature (London) **478**, 360 (2011).

[15] S. Tanzilli, H. De Riedmatten, W. Tittel, H. Zbinden, P. Baldi, M. De Micheli, D. B. Ostrowsky, and N. Gisin, Electron. Lett. **37**, 26 (2001).

[16] E. Brainis, Phys. Rev. A **79**, 023840 (2009).

[17] Q. Lin, F. Yaman, and G. P. Agrawal, Phys. Rev. A **75**, 023803 (2007).

[18] B. Huttner, S. Serulnik, and Y. Ben-Aryeh, Phys. Rev. A **42**, 5594 (1990).

[19] K. J. Blow, R. Loudon, S. J. D. Phoenix, and T. J. Shepherd, Phys. Rev. A **42**, 4102 (1990).

[20] G. Agrawal, *Nonlinear Fiber Optics*, 4th ed. (Academic, Amsterdam, 2006).

[21] Material absorption can be included here and in all the following evolutions by taking z as the effective position in the fiber; $z = \frac{1-e^{-\alpha z'}}{\alpha}$ for absorption coefficient α and true position z'.

[22] B. J. Smith, P. Mahou, O. Cohen, J. S. Lundeen, and I. A. Walmsley, Opt. Express **17**, 23589 (2009).

[23] J. Rarity, J. Fulconis, J. Duligall, W. Wadsworth, and P. Russell, Opt. Express **13**, 534 (2005).

[24] C. Baker and M. Rochette, IEEE Photonics J. **4**, 960 (2012).

[25] R. Ahmad and M. Rochette, Opt. Express **20**, 9572 (2012).

[26] G. Lenz, J. Zimmermann, T. Katsufuji, M. E. Lines, H. Y. Hwang, S. Spälter, R. E. Slusher, S.-W. Cheong, J. Sanghera, and I. D. Aggarwal, Opt. Lett. **25**, 254 (2000).

[27] A. S. Clark, M. J. Collins, A. C. Judge, E. C. Mägi, C. Xiong, and B. J. Eggleton, Opt. Express **20**, 16807 (2012).

[28] Y. Chen, J. Opt. Soc. Am. B **6**, 1986 (1989).